





ARTICLE

Burmese pythons exhibit a transient adaptation to nutrient overload that prevents liver damage

Jason A. Magida^{1,2*}, Yuxiao Tan^{1*} , Christopher E. Wall^{1,2*} , Brooke C. Harrison¹ , Thomas G. Marr³, Angela K. Peter¹, Cecilia A. Riquelme^{1,4}, and Leslie A. Leinwand¹ 

As an opportunistic predator, the Burmese python (*Python molurus bivittatus*) consumes large and infrequent meals, fasting for up to a year. Upon consuming a large meal, the Burmese python exhibits extreme metabolic responses. To define the pathways that regulate these postprandial metabolic responses, we performed a comprehensive profile of plasma metabolites throughout the digestive process. Following ingestion of a meal equivalent to 25% of its body mass, plasma lipoproteins and metabolites, such as chylomicra and bile acids, reach levels observed only in mammalian models of extreme dyslipidemia. Here, we provide evidence for an adaptive response to postprandial nutrient overload by the python liver, a critical site of metabolic homeostasis. The python liver undergoes a substantial increase in mass through proliferative processes, exhibits hepatic steatosis, hyperlipidemia-induced insulin resistance indicated by PEPCK activation and pAKT deactivation, and de novo fatty acid synthesis via FASN activation. This postprandial state is completely reversible. We posit that Burmese pythons evade the permanent hepatic damage associated with these metabolic states in mammals using evolved protective measures to inactivate these pathways. These include a transient activation of hepatic nuclear receptors induced by fatty acids and bile acids, including PPAR and FXR, respectively. The stress-induced p38 MAPK pathway is also transiently activated during the early stages of digestion. Taken together, these data identify a reversible metabolic response to hyperlipidemia by the python liver, only achieved in mammals by pharmacologic intervention. The factors involved in these processes may be relevant to or leveraged for remediating human hepatic pathology.

Introduction

As the principal tissue responsible for regulating metabolic homeostasis, the liver performs a central role in metabolism, including the synthesis, storage, and redistribution of nutrients such as carbohydrates, lipids, and vitamins. Accordingly, severe metabolic perturbations including obesity and type 2 diabetes can lead to permanent hepatic pathologies such as nonalcoholic fatty liver disease (NAFLD; [Lonardo et al., 2005](#)). Promoting liver function by reversing hepatic steatosis and suppressing hepatic gluconeogenesis represents an effective therapeutic strategy for many metabolic diseases ([Petersen et al., 2005](#); [Wada et al., 2010](#)).

Traditional laboratory animal models of metabolic diseases have provided considerable insight into the mechanisms that drive the development of hepatic pathological conditions ([Weltman et al., 1996](#); [Kim et al., 2004](#)). Studying nontraditional animal models that have evolved unique mechanisms to adapt to extreme environmental and metabolic stress should provide valuable information that may lead to interventions in liver

disease in humans. Many such animals exist: certain mammals hibernate for months at a time with no food or water, and some reptiles eat massive meals after extended fasting. Studying animals with extreme biology has led to the development of new drugs. For example, exenatide (Byetta), an antidiabetic drug, was developed from studying the saliva of the infrequently feeding Gila monster lizard, which contains a protein that increases insulin production and islet β -cell proliferation. Although the human protein has too short a half-life to be therapeutic, the Gila monster ortholog, with a much longer half-life, has been marketed since 2005 ([Furman, 2012](#); [Deane et al., 2010](#)).

Among all vertebrates, ectotherm species represented by snakes are dramatically different in terms of metabolic regulation compared with endotherm species represented by mammals. Multiple species of snakes have evolved remarkable mechanisms of metabolic regulation to tolerate periods of feast and famine. One striking example of extreme metabolic

¹Department of Molecular, Cellular, and Developmental Biology and BioFrontiers Institute, University of Colorado, Boulder, CO; ²Gene Expression Laboratory, Salk Institute for Biological Studies, La Jolla, CA; ³Hiberna Corporation, Boulder, CO; ⁴Department of Cell and Molecular Biology, Catholic University of Chile, Santiago, Chile.

*J.A. Magida, Y. Tan, and C.E. Wall contributed equally to this paper. Correspondence to Leslie A. Leinwand: Leslie.Leinwand@colorado.edu.

© 2022 Magida et al. This article is distributed under the terms of an Attribution–Noncommercial–Share Alike–No Mirror Sites license for the first six months after the publication date (see <http://www.rupress.org/terms/>). After six months it is available under a Creative Commons License (Attribution–Noncommercial–Share Alike 4.0 International license, as described at <https://creativecommons.org/licenses/by-nc-sa/4.0/>).

adaptation is the Burmese python (*Python molurus bivittatus*), which has the ability to massively downregulate metabolic rate and physiological functions during extended fasts of up to a year. Upon eating a very large meal, the Burmese python can rapidly increase its metabolic rate to 20–44-fold above fasting levels to process and digest meals that can be in excess of 100% of its body weight (Secor and Diamond, 1995, 1998). Processing meals of this size places a substantial metabolic stress on these animals, which experience a dramatic >100-fold increase in plasma triglyceride (TG) content and subsequent clearance from circulation (Secor and Diamond, 1998; Riquelme et al., 2011). To facilitate this dramatic transition, nearly every organ undergoes a reversible significant adaptive increase in size and function within as little as 1 d post-feeding (1DPF; Secor and Diamond, 1997). For example, python intestines dramatically increase in mass and volume after feeding, including a substantial increase in microvillus area, likely to facilitate nutrient uptake (Lignot et al., 2005; Enok et al., 2016b). In addition, several studies have reported that the python heart undergoes reversible physiologic hypertrophy (Secor and Diamond, 1995, 1998; Andersen et al., 2005; Riquelme et al., 2011). In contrast, another study reported only increased stroke volume, heart rate, and VO_2 (Enok et al., 2013; 2016a). However, only a few studies have investigated the postprandial response of the python liver, despite its massive growth by increasing wet weight by 53% at 3DPF, and the importance of this organ in metabolic homeostasis (Secor and Diamond, 1995). RNA-sequencing analysis of four metabolic organs, including liver, as a function of feeding in the Burmese python was reported (Andrew et al., 2017). The authors reported 711 differentially regulated genes between fasted, 1DPF, and 4DPF livers. Bioinformatics analysis predicted involvement of NRF2, mTOR, Akt, LXR/RXR, and PPAR pathways in the postprandial response of the liver (Andrew et al., 2017). Another liver transcriptome analysis of the Burmese python identified upregulated expression of apolipoproteins and albumin, which indicate increased lipid metabolism (Duan et al., 2017). They also reported increased gene expression associated with an antioxidant response, which is congruent with bioinformatic prediction of the NRF2 pathway activation (Andrew et al., 2017).

Here, we describe the digestive molecular response in the Burmese python that is unparalleled in meal size or metabolite spike magnitude in mammals. While digestive processes in mammals occur over the course of several hours, pythons take ~6–10 d to digest their meals (Secor and Diamond, 1995, 1998). Underscored by dietary TG kinetics, the mammalian postprandial peak of blood TG occurs 3–4 h after meal initiation (Lambert and Parks, 2012), whereas TG levels increase significantly starting a few hours after meal ingestion and remain elevated for days in the python (Riquelme et al., 2011). This is accompanied by substantially increased free fatty acids in circulation and a late-stage elevation in high-density lipoprotein (HDL) cholesterol. In contrast to postprandial mammals (Langsted et al., 2008), the circulating lipid profiles in pythons change minimally in response to normal food intake.

To understand the extreme postprandial metabolic profile and protective strategies of the python, we adopted a metabolomics approach to characterize the digestive resolution period

for the python. Postprandial metabolites in the python plasma included massive increases in bile acids and fatty acids. Correspondingly, bile- and fatty acid-binding nuclear receptors, including farnesoid X receptor (FXR) and peroxisome proliferator-activated receptor (PPAR), were potently activated in the liver. The python liver undergoes significant metabolic activation upon feeding, resulting in cell proliferation, steatosis, transient insulin resistance, and lipogenesis. As all healthy metabolic parameters are defined in mammals, some of these responses would indicate hepatic pathology in mammals, yet they appear to be adaptive hepatic responses in the python, thus revealing novel python biology. Even though these responses of the liver are transient and reversible in postprandial pythons in a matter of days, this process is repetitive throughout the very long lives of pythons. These findings highlight an adaptation by the python liver that demonstrates it to be capable of mitigating transient extreme metabolic activation and then resolving that stress.

Materials and methods

Animals

Burmese pythons were obtained as hatchlings from Strictly Reptiles or Bob Clark Reptiles and housed individually for 6–12 mo at ~30°C on a 10/14 h light/dark cycle. During this period, pythons were fed biweekly meals of intact rats until they grew to 400 g, 750 g, or (for the Metabolon data) 1,250 g. Before collection, pythons were acclimated to three 28-d feeding cycles. Meal-to-body mass ratio was used to quantify food content, and the caloric content was not determined in this study. A sedentary fed male rat is composed of 25.3% protein, 14.6% fat, and 2.9% ash (bone mineral content; Cortright et al., 1997). After the last 28-d fast, pythons were fed rats ~25% of their body mass. Pythons were euthanized at each prandial state (e.g., fasted and 0.25, 0.5, 1, 2, 3, 6, and 10DPF), then tissue and plasma were collected, snap-frozen, and stored at –80°C. All mice were housed in vivarium at ~22°C on a 10/14 h light/dark cycle. Before measuring the plasma TG level, overnight-fasted wild type mice at baseline were fed a 750- μ l bolus of refined corn oil delivered by oral gavage (at 2.5, 7.5, and 24 h). The refined corn oil was composed of ~99% acylglycerols (mono-, di-, and primarily tri-) and ~1% minor lipids such as sterols and tocopherols (Dupont et al., 1990). Wild type, hypercholesterolemic *Ldlr*^{-/-} or leptin-deficient obese *Ldlr*^{-/-} mice were fasted for 6 h before measuring plasma TG level. All procedures were conducted under the approval of the University of Colorado Boulder or the University of Alabama, Tuscaloosa, Institutional Animal Care and Use Committee.

Metabolomics

Liquid chromatography/tandem mass spectrometry analysis of ~200 plasma metabolites was performed on whole python plasma (collected posthumously) by Metabolon. Imputed values for metabolites at each postprandial state were compared and analyzed using MetaboAnalyst (Xia et al., 2015). For this analysis, metabolite concentrations were normalized, log transformed, and scaled through mean-centering and dividing

by the SD of each variable. MetaboAnalyst was subsequently used to conduct and generate the partial least squares discriminant analysis (PLS-DA), volcano plots, and metabolite heatmap.

Enzymatic and colorimetric assays

Plasma alanine aminotransferase (ALT) levels were quantified using a kit from Catechem per manufacturer's instructions. Plasma glucose was measured with a glucose oxidase assay (Cayman Chemical). Glycogen levels from python livers were quantified as glucose released by amyloglucosidase as previously described (Passonneau and Lauderdale, 1974). Plasma and lipoprotein fraction TG and non-esterified free fatty acid content and cholesterol were measured using thin-layer chromatography and commercial kits from Wako Diagnostics (L-type TG H, NEFA-HR 2, and Chol-E) per manufacturer's instructions, and normalized to protein content. Lipoprotein fractions were isolated as previously described (Teupser et al., 2004).

Histologic analysis

For bromodeoxyuridine (BrdU) staining, BrdU was first injected i.p. (4×100 mg/kg at 2-h intervals) after feeding. Python livers were then fixed, sectioned, and stained with a BrdU-specific antibody (Mas 250b; Harlan Sera Laboratories) as we have described previously (Riquelme et al., 2011). For Oil Red O staining, python livers were snap-frozen and imbedded in O.C.T. medium for sectioning. Sections were stained with Oil Red O, then counterstained with hematoxylin. For Picosirius Red staining, python liver was fixed in 10% neutral buffered formalin for sectioning, Picosirius Red staining was performed using standard procedures. From each stained tissue slide, five random fields of view were manually selected and imaged using a Nikon Eclipse Ti-E microscope equipped with a Nikon 0.75 NA (Air) 20 \times objective. Images were analyzed by the color threshold tool in ImageJ (National Institutes of Health).

Lipid thin-layer chromatography

Whole lipids were isolated from python liver tissue or FaO hepatoma cells using a modified Folch extraction and resolved on silica gel G TLC plates as previously described (Magida and Leinwand, 2014). Band intensity was quantified using ImageJ (National Institutes of Health).

Quantitative RT-PCR (qPCR)

Total RNA was isolated from python tissue and cells with TRIzol reagent, and cDNA was subsequently synthesized from 1 μ g of RNA using iScript (Bio-Rad). mRNA levels were quantified with SYBR Green (Bio-Rad). These experiments were performed in triplicate, and expression levels were normalized against Hprt (python) mRNA levels. qPCR primers were designed using recently generated whole genomic and transcriptomic Burmese python sequence libraries (Wall et al., 2011). Sequences for qPCR primers are available in Table S2.

Western blot

Burmese python liver was homogenized in radioimmunoprecipitation assay buffer (#9806; Cell Signaling Technology), supplemented with protease and phosphatase inhibitors cocktail

(#78442; Thermo Fisher Scientific), and centrifuged at 14,000 *g* for 15 min. 10 μ g of protein (python) from the supernatant was resolved by SDS-PAGE and analyzed by Western blot using antibodies from Cell Signaling Technology: p-pASK1 (Thr845; #3765), p-MKK3 (Ser198)/p-MKK6 (Ser207; #12280), p-p38 (Thr180/Tyr182; #4511), p-AKT (Ser473; #4058), and FASN (#3180). Total protein stain (LI-COR #926-11016; Lincoln) was used for Western blot normalization (Figs. S4, C-H; and S5).

Statistical analysis

Statistical analysis was performed with GraphPad Prism 9. Data are represented as mean \pm SEM unless otherwise specified. A two-tailed unpaired Student's *t* test or one-way ANOVA with Bonferroni's multiple comparison was used to determine the significance of differences between data sets. For all cases, differences were considered statistically significant when $P \leq 0.05$.

Online supplemental material

Fig. S1 shows levels of non-esterified fatty acids (NEFAs), TG, cholesterol, and phospholipid in Fasted and 3DPF pythons. Fig. S2 shows alignment of FXR ortholog in human, mouse, chicken, python, and anolis. Fig. S3 shows alignment of PPAR α orthologs in human, mouse, chicken, python, and anolis. Fig. S4 shows ROS level measurement and Western blots used for quantitative analysis and total protein stain normalization showed in Fig. 5. Fig. S5 shows Western blot total protein stain of representative blots showed in Fig. 5 A. Table S1 lists the top 10 conserved domain hits for python FXR and PPAR α orthologs. Table S2 lists sequences of primers used for RT-PCT.

Results

Burmese pythons are protected from postprandial hypertriglyceridemia

After 28 d of fasting, pythons consumed meals representing 25% of their body weight. Their plasma was analyzed for lipids at the following time points: fasted and 0.25, 0.5, 1, 2, 3, 6, and 10DPF. NEFAs increased two- to threefold and remained elevated through 3DPF (Figs. 1 A and S1 A). Plasma TG levels peaked in 2DPF plasma, with an 88-fold increase compared with fasted, reflected by TG content in the chylomicron/ultra-low-density lipoprotein and low-density lipoprotein (LDL) fractions (Fig. 1, B and C; and Table 1). These plasma TG levels in the fed python have been observed in mice only under extreme experimental conditions: either combined leptin and LDL receptor deficiency or after a single, exceedingly large (750 μ l) oral gavage of corn oil (Fig. 1 B).

Although the rodent meal was also cholesterol rich, there was no significant increase in total or LDL cholesterol levels compared with the fasted condition (Fig. 1 D). However, cholesterol in the most buoyant fraction peaked at 2DPF, coinciding with maximal TG content in this fraction. During digestion, mammalian intestines or liver secrete lipid-rich lipoproteins to package TG, while increasing plasma concentration and promoting subsequent TG clearance from plasma (Cohn et al., 1989). Therefore, we measured plasma apolipoprotein B (ApoB), the primary and requisite lipid-rich lipoprotein for packaging

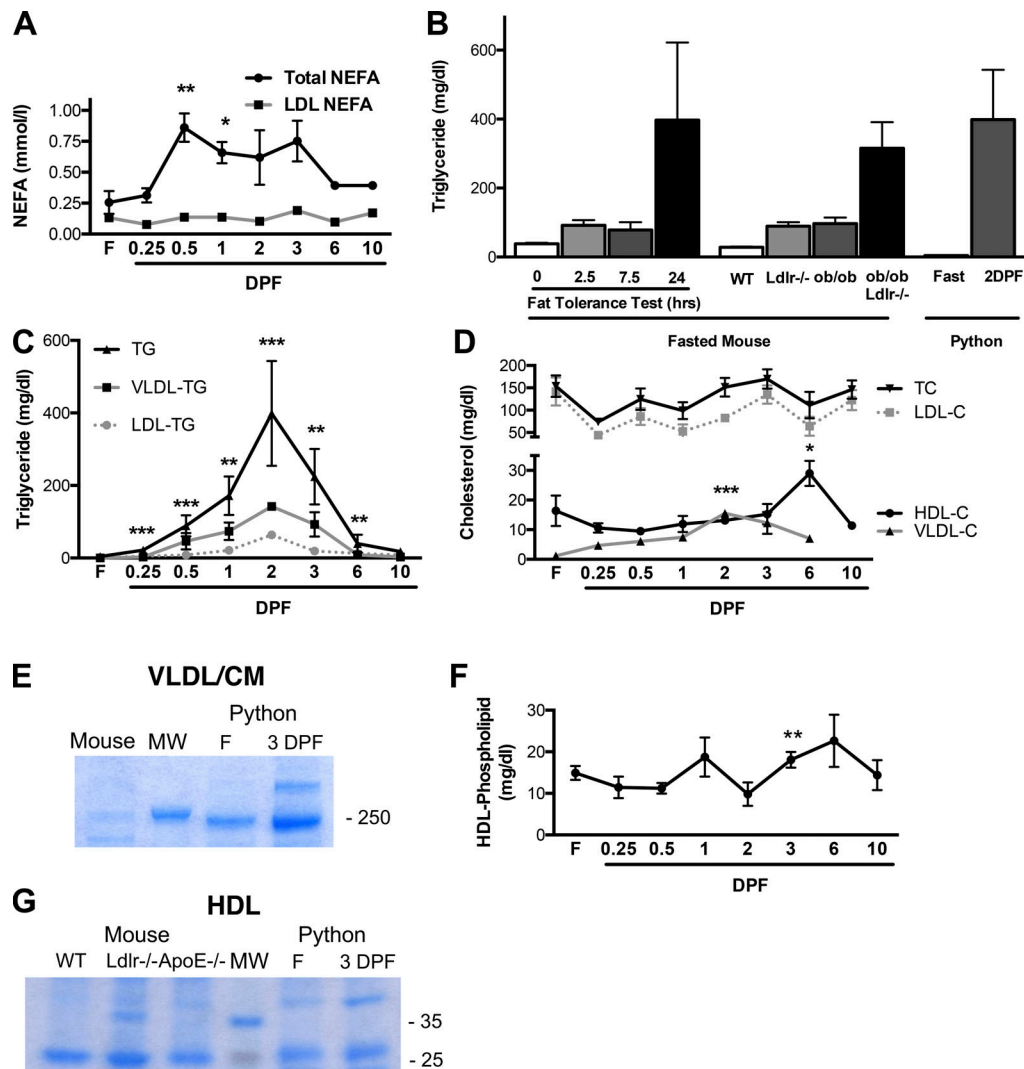


Figure 1. Postprandial hypertriglyceridemia. (A) Plasma NEFA levels, determined by colorimetric enzymatic assay. (B) Comparison of plasma TG in fasted/overnight fasted wild type mice at baseline and after a 0.75-ml bolus of corn oil delivered by oral gavage at 2.5, 7.5, and 24 h; and wild type, hypercholesterolemic *Ldlr*^{-/-} or leptin-deficient obese (*ob/ob*) *Ldlr*^{-/-} mice fasted for 6 h. (C and D) TG and cholesterol concentrations in plasma and isolated VLDL/chylomicron, LDL, and HDL fractions, determined by colorimetric enzymatic assays. (E) Coomassie-stained ApoB levels in the VLDL/chylomicron fraction of wild type C57BL/6 mice and pythons, determined by SDS-PAGE, or pre-stained molecular weight (MW) marker. (F) HDL phospholipid content in pythons, determined by colorimetric enzymatic assay. (G) Coomassie-stained HDL protein from fasted wild type, *Ldlr*, or *ApoE* knockout mice and fasted/fed pythons or MW marker. Data are represented as mean \pm SD. $n = 3/\text{group}$. *, $P \leq 0.05$; **, $P \leq 0.01$; ***, $P \leq 0.001$ versus fasted (F) or WT. Source data are available for this figure: SourceData F1.

chylomicron/VLDL, VLDL, and LDL particles (Cohn et al., 1989). Both main isoforms, ApoB100 and ApoB48, increased during digestion in python plasma (Fig. 1 E). This indicates synchronized coordination of lipid secretion and clearance in python plasma.

Importantly, we observed a 1.8-fold increase in HDL cholesterol at 6DPF, representing the end of digestion and a likely indication of progressive lipid clearance (Fig. 1 D). This occurred independently of increasing the major component of the HDL particle, ApoA1 (~27 kD), in the HDL fraction. Meanwhile, the levels of the orthologous cholesterol-acceptor remained unchanged throughout our selected postprandial digestion time points in the python. The other putative orthologue of ApoE (~36–38 kD) appeared in the HDL fraction at 2DPF, peaking

between 3 and 6DPF (Fig. 1 G). Lastly, HDL phospholipid content remained largely steady, at ~20 mg/dl (Fig. 1 F).

As we observed spikes of different lipid content at various time points at extreme levels compared to mammalian models, lipid-rich lipoproteins increased coordinately to promote lipid clearance from plasma. Therefore, this highly dynamically regulated process is likely an indication of protective collaboration among multiple metabolic tissues to maintain metabolic homeostasis in the python.

Distinct postprandial metabolomic states in Burmese pythons

Surges of various lipid contents across the course of digestion led us to analyze the postprandial metabolic response in python plasma at three time points: fasted, 1DPF, and 3DPF. We used

Table 1. Circulating metabolic parameters in the python

Item	Plasma concentration (mg/dl)			
	Fasted	1DPF	3DPF	10DPF
Glucose	31.7 ± 14.5	44.1 ± 2.4	33.7 ± 16.2	24.4 ± 10.4
Total TG	4.5 ± 0.7	171.7 ± 53.0	224.1 ± 76.7	17.5 ± 0.5
VLDL/chylomicron TG	ND	73.6 ± 24.1	75.3 ± 31.1	2.7 ± 0.0
LDL TG	0.8 ± 0.7	21.2 ± 9.1	19.9 ± 0.3	8.0 ± 1.6
Total cholesterol	153.7 ± 23.9	99.0 ± 18.7	169.9 ± 21.7	111.3 ± 29.8
VLDL cholesterol	1.2 ± 0.1	7.4 ± 1.2	12.3 ± 3.8	5.8 ± 1.3
LDL cholesterol	141.7 ± 31.2	52.8 ± 15.7	135.0 ± 20.3	122.7 ± 22.5
HDL cholesterol	16.4 ± 5.1	11.9 ± 2.7	15.2 ± 3.4	11.4 ± 0.4

statistical clustering to compare relative levels of lipids and amino acids (as defined by metabolite superpathways) that differentiate the three states in a heatmap (Fig. 2, A and B). For this analysis, we analyzed five representative animals in each group. Interestingly, a unique cluster of lipids and amino acids emerged at each postprandial time point. Separate clusters of amino acids were most evident, especially at 3DPF. These findings provide evidence for distinct postprandial metabolic states throughout early digestion in pythons.

Roughly 200 distinct metabolites were identified as differentially present between each of these postprandial states, including lipids, amino acids, and carbohydrates. Principle component-based PLS-DA of these metabolites revealed that the global metabolomic profiles for fasted, 1DPF, and 3DPF are largely distinct (Fig. 2, A–C). Corresponding volcano plots identified metabolites that are most differentially regulated at 1DPF or 3DPF relative to fasted (Fig. 2, D and E).

From here, we focused on important metabolites that might define each postprandial state. Despite the snake having consumed a carcass, which constitutes a cholesterol-rich meal, metabolomic analysis indicated no alteration in plasma total cholesterol (Fig. 3 A), consistent with our comprehensive enzymatic determinations. The cholesterol precursor 7-dehydrocholesterol and the bile acids taurocholate and taurochenodeoxycholate were increased 86.4- and 66.7-fold after feeding, respectively (Fig. 3, B and C). The importance of this postprandial plasma bile acid spike is supported by an in silico sequence analysis of the python bile acid-sensing FXR (NRIH4). It exhibits a high (98.3%) phylogenetic conservation of dimer interface as well as DNA, zinc, and ligand-binding sites with that of mammals (i.e., mouse and human; Fig. S2). In fact, the top hit in an in silico conserved domain query for the Burmese python FXR sequence was the FXR ligand-binding domain (E -value = 6.2×10^{-141} ; Table S1). Consistent with increased bile acid-mediated regulation of transcription through FXR, we found activation of bile acid-induced FXR (NRIH4) and FGF19 expression, as well as the repression of CYP7A1 mRNA at 1DPF, responsible for catalyzing the initial step in bile acid biosynthesis from cholesterol precursors (Fig. 3 D). FGF19 and CYP7A1 are canonical positively and negatively regulated FXR targets, respectively.

Digestive hepatic metabolic responses to feeding in Burmese pythons

Striking postprandial increases in plasma metabolites, including bile acids and fatty acids, led us to examine the metabolic consequences of digestion in the liver. The liver plays a key role in metabolic homeostasis. Therefore, we assayed markers of hepatic damage known to be induced by nutrient overload in mammals. At 1DPF, plasma ALT activity exceeded 100 U/liter (Fig. 4 A), nearly fourfold higher than the upper limit considered to be normal in mammals, 30 U/liter for women and 40 U/liter for men (Prati et al., 2002). After 3DPF, ALT activity subsequently decreased throughout the course of digestion, returning to near-fasting levels by 10DPF, representing the end of digestion (Fig. 4 A). Further supportive of transient hepatosteatosis was increased Oil Red O staining of neutral lipids in the liver at 3DPF (Fig. 4 C). In addition, upregulated Colla expression and Picrosirius Red staining indicate increased hepatic fibrosis, also at 3DPF (Fig. 4, B, F, and G). These conditions regressed and returned to fasted levels by 10DPF (Fig. 4, B and C). Increased hepatic TG storage was demonstrated by chromatographic separation of total lipids from the liver (Fig. 4, D and E). Similar to plasma cholesterol content, hepatic cholesterol levels were not elevated after feeding (Fig. 4 D). Hepatic uptake, trafficking, and catabolism of fats, bile acids, and cholesterol are largely coordinated through transcriptional regulation of metabolic gene expression via the nuclear receptors PPAR and FXR (Kersten et al., 2000). PPAR α and PPAR γ expression have been reported to be upregulated by 2.2-fold and 0.6-fold in 1DPF Burmese pythons, respectively (Andrew et al., 2017). Like FXR, the python PPAR α dimer, DNA, zinc, and ligand-binding sites were found to be exceptionally well conserved in other more closely related species (e.g., chicken and anolis lizard) as well as mammals (e.g., human and mouse). The greatest sequence homology to the PPAR ligand and DNA-binding domains displayed an E value = 1.4×10^{-134} for closely related species and an E value = 1.3×10^{-56} for mammals (Fig. S3 and Table S1). In accordance with the conservation of PPAR α functional sites and postprandial hyperlipidemia, we observed a dramatic, but reversible, hepatic upregulation of several canonical PPAR α target genes involved in fatty acid clearance and oxidation (Fig. 4 M). Among the hepatic PPAR α targets substantially upregulated was

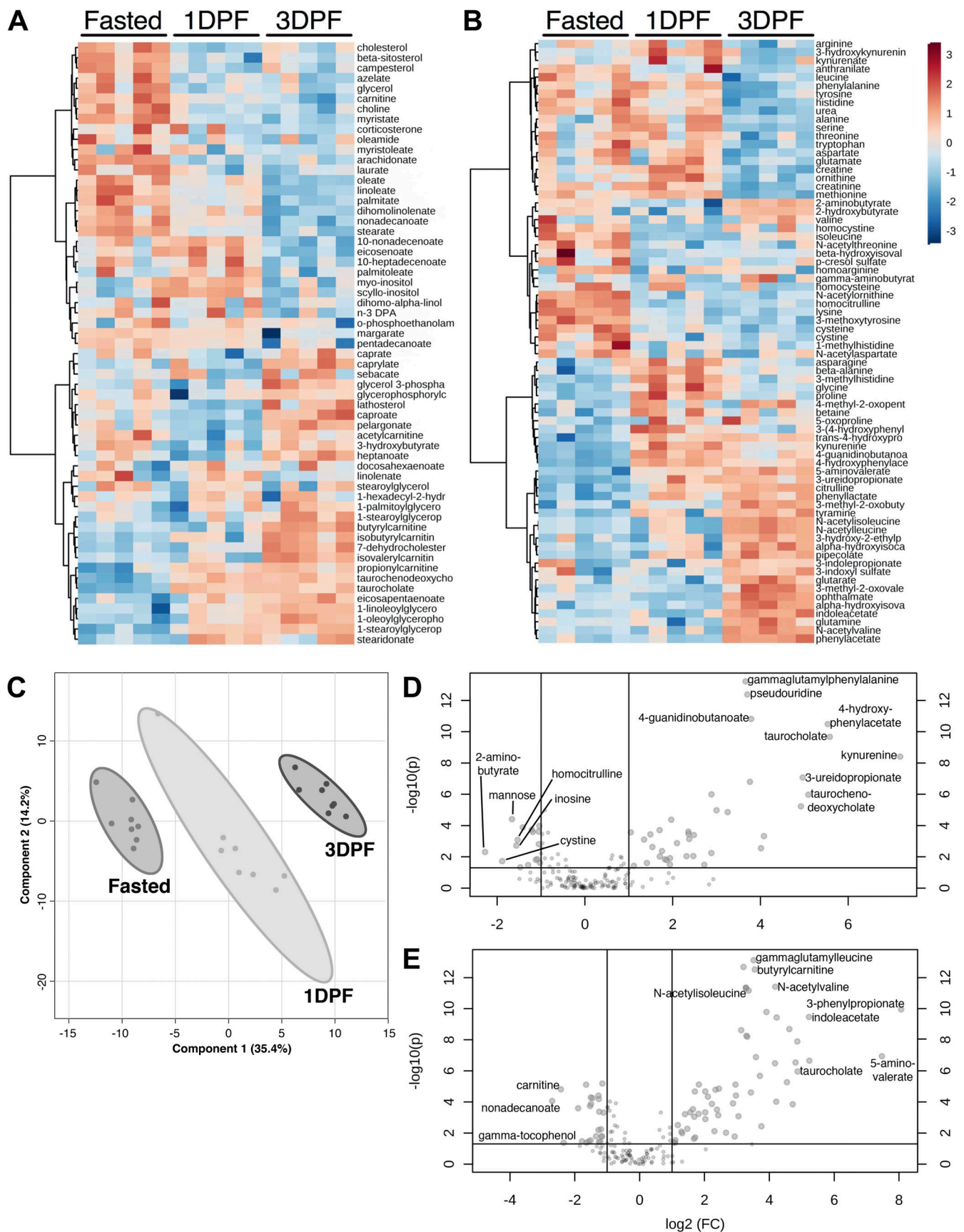


Figure 2. **Emergence of distinguishing metabolite superpathways throughout digestion. (A and B)** Heatmap displaying the rank-ordered levels of differentially regulated plasma: lipid (A) and amino acid (B) metabolites in fasted, 1DPF, and 3DPF Burmese pythons. The differences are \log_2 normalized and

clustered by pattern of regulation between each state. For each state, $n = 5/\text{group}$. **(C)** PLS-DA of two component groups of plasma metabolites that are significantly different between feeding states in Burmese pythons. Each dot represents the metabolome of an individual animal. **(D and E)** Volcano plots for differentially expressed circulating metabolites at 1DPF (D) and 3DPF (E) versus fasted. The \log_2 of the fold-change (FC) for each metabolite (gray dots) is on the x axis, and the $-\log_{10}$ of the P value of this difference is on the y axis.

stearoyl-CoA desaturase, responsible for introducing a double bond into the aliphatic chain of long-chain saturated fatty acids. This double bond formation would significantly alter the hepatic lipid landscape, leading to TG biosynthesis and accumulation. This was supported by the above increase in TG levels and an $\sim 60\%$ increase in the hepatic desaturation index, as determined by gas chromatography (Fig. 4 H).

Other than promoting lipid clearance, there are conditions consistent with hyperlipidemia-induced insulin resistance in the postprandial python: (1) increases in hepatic glycogen content; (2) induction of phosphoenolpyruvate carboxykinase (PEPCK) mRNA, responsible for catalyzing the initial and rate limiting step in gluconeogenesis (Fig. 4, I and J; Yoon et al., 2001). However, while hepatic glycogen levels increased, plasma glucose levels in the python remain not only low, but steady at ~ 40 mg/dl (Fig. 4 K and Table 1). Collectively, these findings suggest that postprandial python livers exhibit metabolic activation and transient cellular responses in early digestion stage, including steatosis, hyperlipidemia-induced insulin resistance along with PEPCK activation.

Digestive hepatic responses to feeding in Burmese pythons

Parallel to transcriptional programs of metabolic gene expression regulated by PPAR α and FXR, stress responses in mammals usually involve coordinated posttranslational activation of MAPK signaling. p38 MAPK is a stress-kinase signaling pathway

critical to hepatic metabolism. However, reduced activity in *ob/ob* and high fat diet-fed obese mice has been observed (Lawan and Bennett, 2017). At 1DPF, the hepatic p38 stress kinase pathway is strongly and transiently activated but is rapidly reduced by 3DPF (Figs. 5, A and B; and S4 A). ASK1 (MAP3K5) and MKK3 (MAP2K3), which mediate the phosphorylation of p38 MAPK, are similarly activated early after feeding (Figs. 5, A and B; and S4 A). Consistent with metabolic substrate content and activity overload, reactive oxygen species (ROS) could represent a likely stress stimulus in the fed python. In the mammalian liver, high plasma lipid content leads to increased ROS production, inducing subsequent tissue damage (Vergara et al., 2019). However, hepatic ROS levels did not change across the digestion time points, suggesting a strong underlying antioxidant mechanism that neutralizes ROS (Fig. S4 B). This is supported by an RNA-sequencing analysis of livers in the Burmese python, which points to an early postprandial activation of the NRF2 pathway, consistent with an antioxidant response (Andrew et al., 2017).

To further investigate whether postprandial Burmese pythons show any signs of hyperlipidemia-induced insulin resistance, the phosphorylation of AKT was tested. At 1DPF, hepatic pAKT is significantly dephosphorylated and further dephosphorylated at 3DPF (Figs. 5, A and C; and S4 A). This signaling is a canonical negative regulator of PEPCK expression. The striking reduction of AKT phosphorylation supports the stated

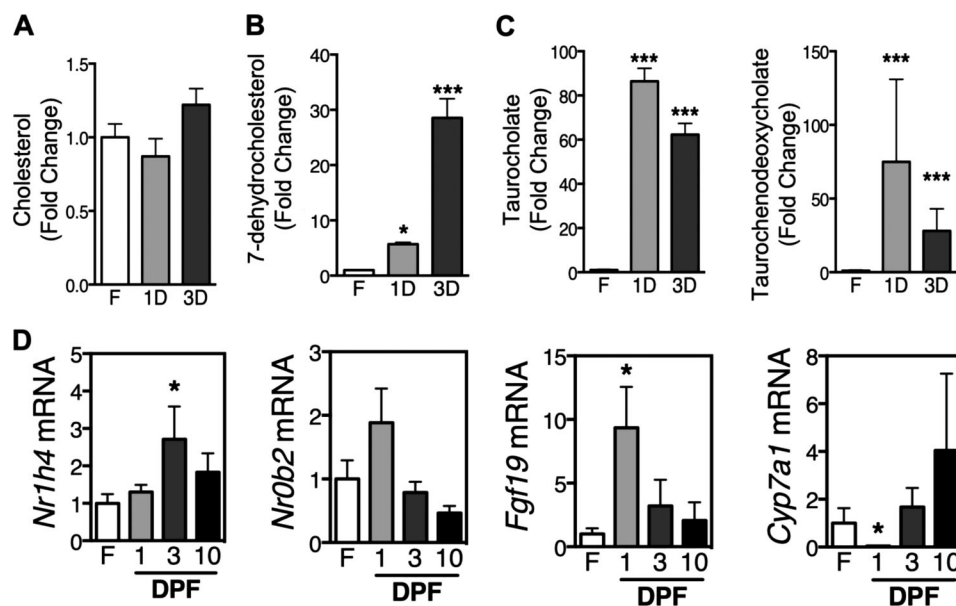


Figure 3. **Postprandial elevation in plasma bile acids and activation of the bile acid receptor in the liver.** **(A–C)** Fold-changes in plasma levels of cholesterol (A), 7-dehydrocholesterol (B), and taurocholate and taurodeoxycholate (C). **(D)** qPCR for normalized *Nr1h4* (*Fxr*), *Nr0b2* (*Shp*), *Fgf19*, and *Cyp7a1* mRNA expression in fasted (F), 1, 3, and 10DPF python livers. Data are represented as mean \pm SEM. $n = 8/\text{group}$. *, $P \leq 0.05$; **, $P \leq 0.01$; ***, $P \leq 0.001$ versus fasted (F) unless stated otherwise.

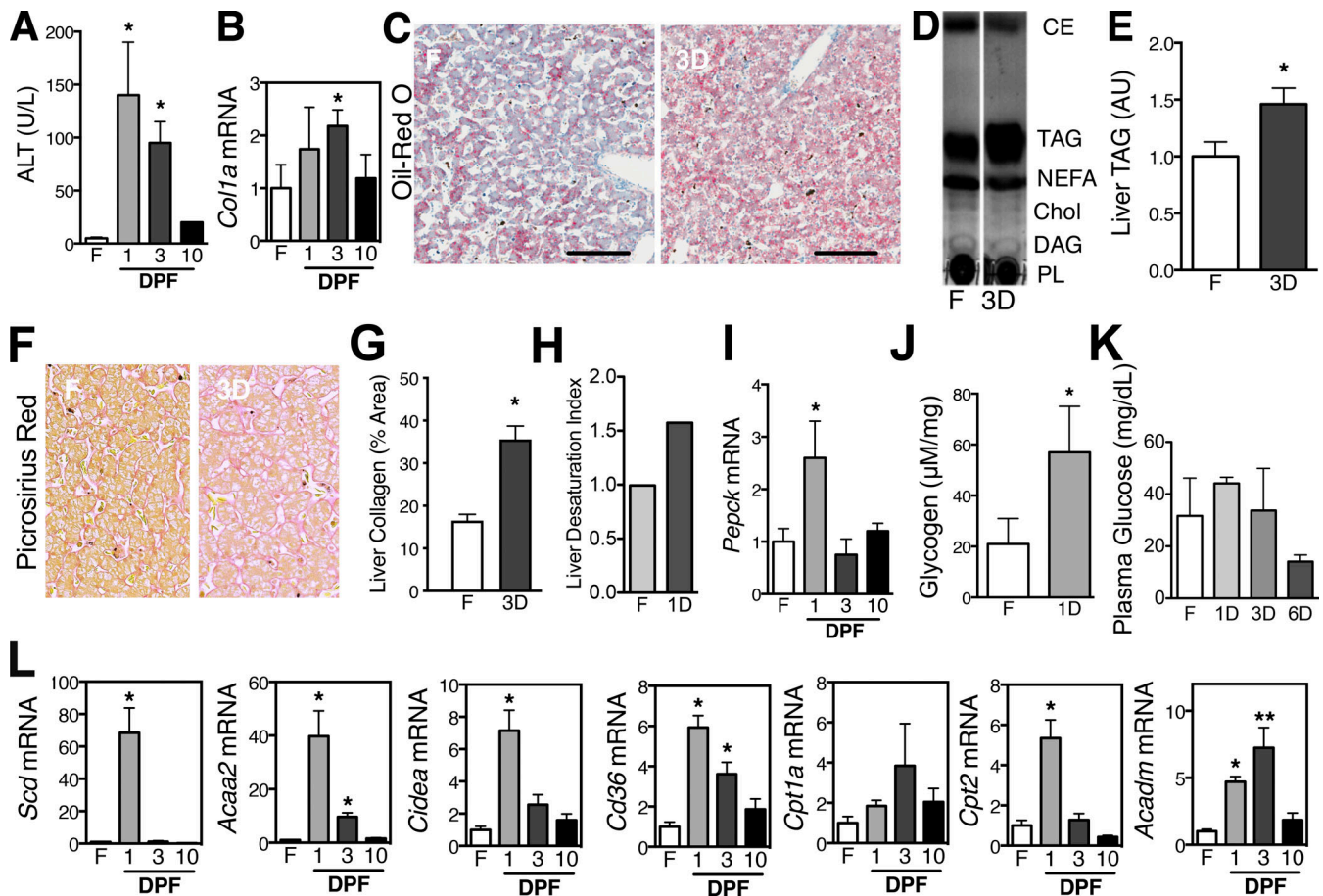


Figure 4. **Transient steatosis, fibrosis, and metabolic activation in the postprandial python liver.** (A) ALT assay (U/liter) in fasted (F), 1, 3, and 10DPF python plasma. (B) Hepatic collagen1 mRNA expression, determined by qRT-PCR. (C) Oil Red O staining of frozen tissue sections from fasted (F) and 3DPF (3D) python livers. Scale bar, 50 µm. (D) Thin-layer chromatography of pooled total lipids extracted from fasted and 3DPF python plasma. CE, cholesterol esters; Chol, free cholesterol; DAG, diacylglycerol; PL, phospholipids; TAG, triglycerides. (E) Quantification of liver triglyceride (TAG) content (arbitrary units, AU) in fasted and 3DPF pythons. (F) Picrosirius red staining of fixed tissue sections from fasted and 3DPF python livers. (G) Quantification of hepatic collagen percentage area in fasted and 3DPF pythons. (H) Hepatic desaturation index of C18 species, determined by gas chromatography. (I) qPCR for *Pepck* mRNA expression in python livers. (J) Assay for glucose derived from glycogen in fasted and 1DPF (1D) python livers. (K) Plasma glucose levels, determined by colorimetric enzymatic assay. (L) qPCR for normalized PPAR target gene (*Acaa2*, acetyl CoA acyltransferase; *Cidea*, cell death-inducing DFFA-like effector A; *Cd36*, fatty acid translocase; *Cpt2*, carnitine palmitoyl transferase; *Scd*, stearyl CoA desaturase) mRNA expression. Data are represented as mean ± SEM. *n* = 3/group. *, *P* ≤ 0.05; **, *P* ≤ 0.01 versus fasted.

supposition that the python liver experiences robust yet reversible insulin resistance, as we observed recovery of pAKT signaling at 10DPF (Figs. 5 A and S4 A).

Along with the transient insulin resistance at an early stage of digestion, strong activation of FASN at 1DPF is consistent with de novo fatty acid synthesis (Figs. 5, A and C; and S4 A). Robust SREBF1/2 activation has also been observed in 1DPF Burmese python liver (Andrew et al., 2017). This marks activation of lipogenesis and is reflected by the significant increase in lipid deposition in 3DPF python liver (Fig. 4, C-E). Hepatic de novo lipogenesis is an important regulator of intrahepatic TG content. A larger contribution of hepatic de novo lipogenesis to hepatic TG deposition has been found in individuals with obesity and NAFLD (Smith et al., 2020). However, these hepatic findings in the snake resolve with no evidence of persistence.

In addition to the pathological effects of p38 MAPK activity, p38 has also been shown to be critical to liver regeneration and

protection against hepatic oxidative stress (Rius-Pérez et al., 2019). Because of plasma lipid overload and the increase in liver mass postprandially (Secor, 2008; Secor and Diamond, 1997, 1998, 1995), we assessed the mechanisms underlying postprandial liver growth. To evaluate potential hyperplastic processes, we observed a threefold increase in hepatocellular BrdU incorporation and a transient fourfold increase in expression of proliferating cell nuclear antigen, indicating active DNA replication (Fig. 5, D-F).

Discussion

The Burmese python is a unique animal model of extreme metabolic regulation, but many questions remain to be addressed, including (1) the nature of its metabolic response to digestion and (2) its ability to accommodate unparalleled postprandial dietary lipid load. In this report, we applied both classic

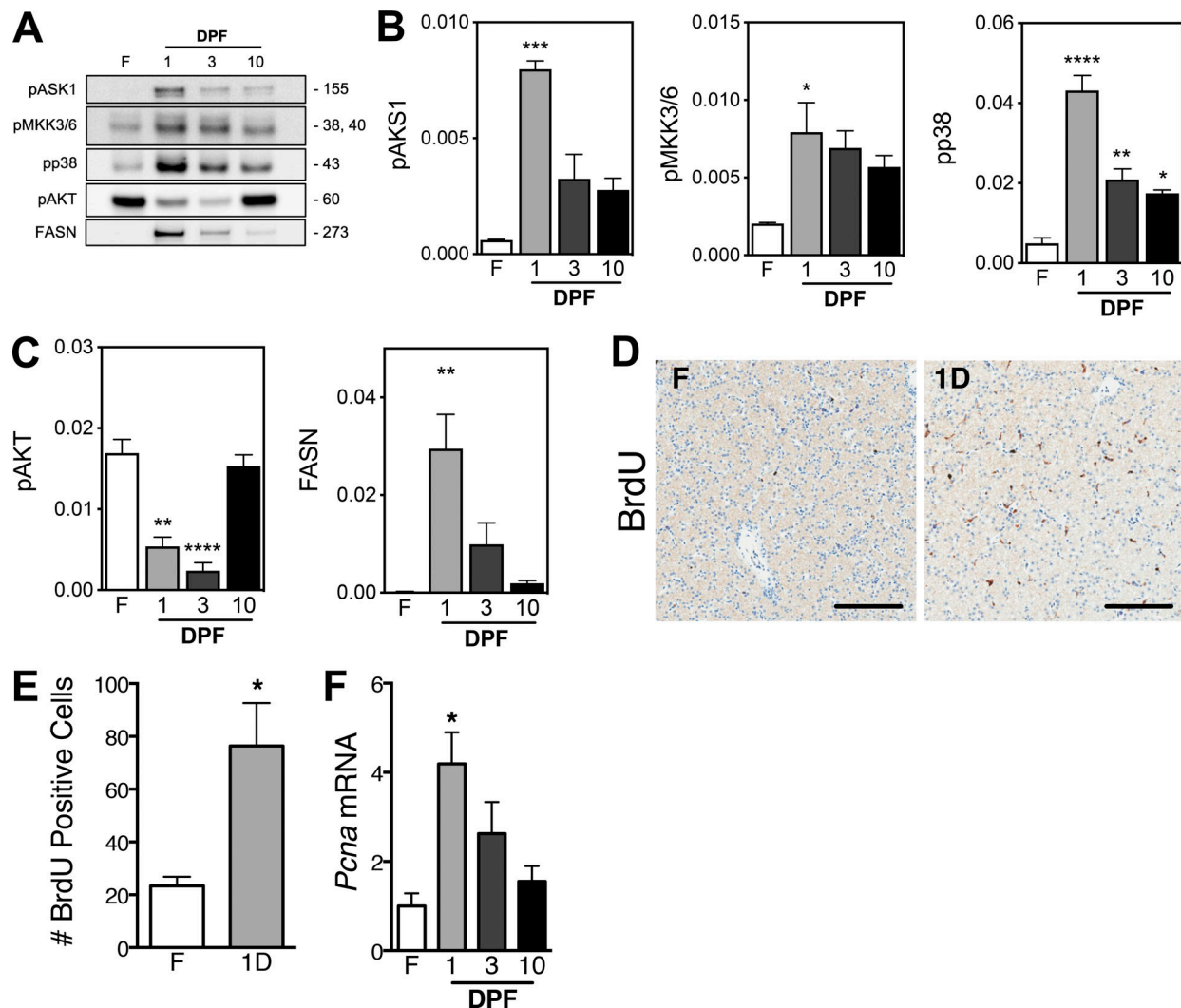


Figure 5. **Transient adaptive responses in the postprandial python liver.** (A and B) Western blot analysis reveals normalized MAPK stress kinase activation of ASK1, MKK3/6, and p38. (C) Western blot analysis indicates normalized AKT deactivation and FASN activation. (D) Immunohistochemical staining for BrdU incorporation into fasted (F) and 1DPF (1D) python livers. Scale bar, 50 μ m. (E) Quantification of BrdU-positive cell numbers per stained fasted and 1DPF python liver sections. (F) qPCR for normalized *Pcna* (proliferating cell nuclear antigen) mRNA expression in fasted and 1, 3, and 10DPF python livers. Data are represented as mean \pm SEM. $n = 3$ /group. *, $P \leq 0.05$; **, $P \leq 0.01$; ***, $P \leq 0.001$; ****, $P \leq 0.0001$ versus fasted. Source data are available for this figure: SourceData F5.

and metabolomic approaches to evaluate the diverse metabolic states present in pythons at different time points during digestion. It has been demonstrated that processing large meals causes dramatic, but reversible, organ growth in pythons, such as intestinal growth and physiologic cardiac hypertrophy (Secor and Diamond, 1998; Andersen et al., 2005; Riquelme et al., 2011). We show here that the python liver exhibits a remarkable and reversible adaptive response to nutrient overload and metabolite flux. At the initial stages of digestion, the python liver tolerates transient postprandial increases in stress markers and stimuli identified in mammalian liver disease, including hepatic steatosis and what appears to be hyperplasia.

During evolution, Burmese pythons developed the unique fasting/feeding paradigm that they use today. In comparison to mammals, Burmese pythons also exhibit an unparalleled circulating plasma composition in addition to the physiological

changes described above. Lipids are a predominant metabolite in circulation after feeding in pythons, where we observed peak TG level at 2DPF, with an 88-fold increase compared with fasted. Comparable plasma TG levels in most mammals would result in lipid deposition in nonadipose tissues such as the heart, which is a pathological condition (Khan et al., 2010). We previously identified three fatty acids that induce physiological cardiac hypertrophy in pythons and mice and in isolated rat cardiac myocytes (Riquelme et al., 2011). Despite the high levels of plasma lipids, no significant increase in total or LDL cholesterol was observed in postprandial python plasma (Fig. 1 D). It would be informative to know the turnover rate of TG and glycogen in both liver and plasma. However, we have been unable to perform interventions in the snakes and have not been allowed to administer radiolabeled TG precursors to snakes. Additionally, glucose was not increased compared with fasted python plasma.

To determine which metabolites were altered in the postprandial plasma compared with fasted and therefore might be responsible for regulating the hepatic response, we assessed how the postprandial metabolome might impact the liver.

While the liver might buffer against sudden TG surges during digestion, products of TG breakdown, including diacylglycerol and free fatty acids, are highly bioactive signaling molecules, as well as energetic substrates. The fact that the postprandial liver remains free of excess diacylglycerol accumulation following a meal, despite unparalleled hyperlipidemia, supports the presence of protective processes that mitigate lipotoxic stimuli and warrant further study. Various fatty acids emerged in abundance at 1DPF from our metabolomic profiling of python plasma. The fact that PPAR α is activated by long-chain fatty acids (Georgiadi and Kersten, 2012), and that fatty acids were found at high levels at 1DPF, coupled with the induction of PPAR α target genes at this time point, implicates a role of PPAR α in the hepatic digestive response. As a transcriptional regulator of fatty acid handling and catabolism genes, PPAR α appears to coordinate the mammalian hepatic response to dietary lipids (Contreras et al., 2013). As expected, we observed a number of the highly induced PPAR α target genes at 1DPF involved in performing essential roles in fatty acid oxidation (e.g., *Acaa2* and *Cpt2*).

Our metabolomics analysis identified additional prominent spikes in plasma analytes during the digestive period in pythons, including the bile acids taurocholate and taurochenodeoxycholate. They are distinguished not only by the striking magnitude of their increases, but also by their proliferation-modulating and anti-inflammatory properties. These bile acids may mitigate pathological facets of hypertriglyceridemia by activating the bile acid receptors FXR/NR1H4 and TGR5 (Chiang and Ferrell, 2020). Indeed, transient FXR activation supports a putative protective role for these bile acids in the postprandial resolution of lipemia and general metabolic stress.

While the importance of PPAR α and FXR activities in the postprandial python liver are apparent, the role of many other metabolites in this response is less clear. One of the more perplexing energetic substrates is glucose, which is present at exceedingly low levels in plasma and does not appear to be altered throughout the digestive process. This pattern of regulation differs from normal postprandial hyperglycemia in mammals but could be attributed to the low glycemic index of the meal, a significant increase in plasma insulin levels present well before 1DPF, or maintenance of newly formed glucose as hepatic glycogen (Secor, 2008). The differences between a lipid-induced gluconeogenic response in mammal and python are underscored by high levels of plasma 3-methyl-2-oxovalerate in the fed python, which has been identified in humans as the strongest predictor of impaired fasting glucose levels (Menni et al., 2013). Indeed, our study demonstrates a disconnect between the fibroproliferative and hyperglycemic outcomes of hepatic lipid overload conferred by the digestive milieu of the Burmese python.

With the surging levels of lipids in the postprandial python, lipid clearance was likely promoted by increased lipid-rich lipoproteins in plasma and upregulated PPAR α target genes involved in fatty acid clearance and oxidation. There are also conditions consistent with hyperlipidemia-induced insulin

resistance in the postprandial python, including deactivation of AKT signaling and upregulated PEPCK expression. These results are consistent with diabetic mice that manifest selective hepatic insulin resistance: insulin fails to block gluconeogenesis (i.e., it loses its ability to suppress PEPCK) but continues to stimulate lipogenesis (i.e., enhanced FASN activation; Brown and Goldstein, 2008; Li et al., 2010). The paradox of selective hepatic insulin resistance has also been identified in a clinical study involving individuals with obesity and NAFLD (Vatner et al., 2015). The Burmese python seems to have evolved solutions for the paradoxical metabolic regulation, and python adipose tissue is likely to play a crucial role in conserving plasma lipids as an energy reservoir. More studies need to be conducted in adipose tissue and intra-organ signaling to understand the extreme postprandial physiology in Burmese pythons.

Finally, as pythons have to accommodate massive meal sizes and the subsequent nutrient overload in the body, we demonstrate a transient response of p38 activation in python liver, and the upstream MAPK stress pathway was activated at 1DPF and then inactivated in the course of digestion. In the past, studies showed reduced hepatic p38 MAPK phosphorylation in *ob/ob* and high fat diet-fed obese mice, whereas activation of p38 by expression of constitutively MKK6 reduced ER stress and maintained euglycemia in obese and diabetic mice (Lee et al., 2011). Furthermore, studies focusing on MKP-1, a phosphatase of p38, demonstrated that MKP-1 plays an important role in the dephosphorylation of p38 MAPK to negatively regulate hepatic TG metabolism and the management of lipid homeostasis (Flach et al., 2011). A recent study further supported the protective role of p38 in hepatocytes that mild stress such as a high fat diet or early stage of hepatic steatosis promotes hepatic function in metabolizing fatty acids. Activation of p38 facilitates β -oxidation, thereby reducing TG storage and load in the liver (Hwang et al., 2020). These conditions and results align with our observations in postprandial pythons: plasma TG content dramatically increases during early stages of digestion, and p38 is activated with elevated β -oxidation gene expression (e.g., *Acaca2*, *Acadm*, and *cpt1/2*). Commonly, activation of p38 is thought to initiate apoptosis. However, the above studies and our results demonstrate different signaling of p38 MAPK in hepatic metabolism.

This study highlights notable metabolic distinctions between reptile and mammalian physiology. What can constitute liver disease in mammals is instead a normal and recurrent digestive process that is rapidly reversible in Burmese pythons. While future studies will be required to elucidate the relative importance of the many other metabolites and corresponding cellular signaling pathways during digestion, our study at present offers a promising first look at metabolic biology in postprandial Burmese pythons, that may be able to exploit to develop hepatic therapeutics to combat liver disease.

Acknowledgments

David A. Eisner served as editor.

We acknowledge the generous provision of some of the python samples used in this study by Prof. S. Secor, University of Alabama, Tuscaloosa, Tuscaloosa, AL.

This work was supported by National Institutes of Health grant R01 GM029090 and by Leducq Foundation grant 21CVD02 (to L.A. Leinwand).

L.A. Leinwand, T.G. Marr, and B.C. Harrison are on the scientific advisory board of, and are shareholders in, Hiberna Corporation, a company that is developing drugs based on natural models of extreme metabolic regulation. C.A. Riquelme is a shareholder in Hiberna Corporation. The remaining authors declare no competing financial interests.

Author contributions; J.A. Magida, Y. Tan, and C.E. Wall coordinated the study and wrote the paper. L.A. Leinwand edited the manuscript. C.E. Wall and B.C. Harrison performed qPCR, C.E. Wall analyzed metabolomics data, Y. Tan performed Western blot analysis, and J.A. Magida carried out the remaining experiments and analysis.

Submitted: 9 August 2021

Revised: 18 January 2022

Accepted: 14 February 2022

References

- Andersen, J.B., B.C. Rourke, V.J. Caiozzo, A.F. Bennett, and J. W. Hicks. 2005. Physiology: Postprandial cardiac hypertrophy in pythons. *Nature*. 434: 37–38. <https://doi.org/10.1038/434037a>
- Andrew, A.L., B.W. Perry, D.C. Card, D.R. Schield, R.P. Ruggiero, S.E. McGaugh, A. Choudhary, S.M. Secor, and T.A. Castoe. 2017. Growth and stress response mechanisms underlying post-feeding regenerative organ growth in the Burmese python. *BMC Genom.* 18:338. <https://doi.org/10.1186/s12864-017-3743-1>
- Brown, M.S., and J.L. Goldstein. 2008. Selective versus total insulin resistance: A pathogenic paradox. *Cell Metab.* 7:95–96. <https://doi.org/10.1016/j.cmet.2007.12.009>
- Chiang, J.Y.L., and J.M. Ferrell. 2020. Bile acid receptors FXR and TGR5 signaling in fatty liver diseases and therapy. *Am. J. Physiol. Gastrointest. Liver Physiol.* 318:G554–G573. <https://doi.org/10.1152/ajpgi.00223.2019>
- Cohn, J.S., J.R. McNamara, S.D. Krasinski, R.M. Russell, and E.J. Schaefer. 1989. Role of triglyceride-rich lipoproteins from the liver and intestine in the etiology of postprandial peaks in plasma triglyceride concentration. *Metabolism*. 38:484–490. [https://doi.org/10.1016/0026-0495\(89\)90203-5](https://doi.org/10.1016/0026-0495(89)90203-5)
- Contreras, A.V., N. Torres, and A.R. Tovar. 2013. PPAR- α as a key nutritional and environmental sensor for metabolic adaptation. *Adv. Nutr.* 4: 439–452. <https://doi.org/10.3945/an.113.003798>
- Cortright, R.N., M.P. Chandler, P.W.R. Lemon, and S.E. Dicarolo. 1997. Daily exercise reduces fat, protein and body mass in male but not female rats. *Physiol. Behav.* 62:105–111. [https://doi.org/10.1016/s0031-9384\(97\)00148-0](https://doi.org/10.1016/s0031-9384(97)00148-0)
- Deane, A.M., M.J. Chapman, and M. Horowitz. 2010. The therapeutic potential of a venomous lizard: The use of glucagon-like peptide-1 analogues in the critically ill. *Crit. Care*. 14:1004. <https://doi.org/10.1186/cc9281>
- Duan, J., K.W. Sanggaard, L. Schauser, S.E. Lauridsen, J.J. Enghild, M.H. Schierup, and T. Wang. 2017. Transcriptome analysis of the response of Burmese python to digestion. *Gigascience*. 6:1–18. <https://doi.org/10.1093/gigascience/gix057>
- Dupont, J., P.J. White, M.P. Carpenter, E.J. Schaefer, S.N. Meydani, C.E. Elson, M. Woods, and S.L. Gorbach. 1990. Food uses and health effects of corn oil. *J. Am. Coll. Nutr.* 9:438–470. <https://doi.org/10.1080/07315724.1990.10720403>
- Enok, S., L.S. Simonsen, and T. Wang. 2013. The contribution of gastric digestion and ingestion of amino acids on the postprandial rise in oxygen consumption, heart rate and growth of visceral organs in pythons. *Comp. Biochem. Physiol. - Part A. Mol. Integr. Physiol.* 165:46–53. <https://doi.org/10.1016/j.cbpa.2013.01.022>
- Enok, S., G.S.P.C. Leite, C.A.C. Leite, H. Gesser, M.S. Hedrick, and T. Wang. 2016a. Improved cardiac filling facilitates the postprandial elevation of stroke volume in Python regius. *J. Exp. Biol.* 219:3009–3018. <https://doi.org/10.1242/jeb.142729>

- Enok, S., L. Staerdal Simonsen, P. Funch, A. Kruse, J. Frederik Dahlerup, and T. Wang. 2016b. Digestive physiology in reptiles with special reference to pythons. In *Amphibian and Reptile Adaptation to the Environment: Interplay between Physiology and Behavior*. C.R. Bevier, D.V. de Andrade, and J.E. de Carvalho, editors. CRC Press. 81–113. <https://doi.org/10.1201/b20420>
- Flach, R.J.R., H. Qin, L. Zhang, and A.M. Bennett. 2011. Loss of mitogen-activated protein kinase phosphatase-1 protects from hepatic steatosis by repression of cell death-inducing DNA fragmentation factor A (DFFA)-like effector C (CIDE)/fat-specific protein 27. *J. Biol. Chem.* 286: 22195–22202. <https://doi.org/10.1074/jbc.M110.210237>
- Furman, B.L. 2012. The development of Byetta (exenatide) from the venom of the Gila monster as an anti-diabetic agent. *Toxicol.* 59:464–471. <https://doi.org/10.1016/j.toxicol.2010.12.016>
- Georgiadi, A., and S. Kersten. 2012. Mechanisms of gene regulation by fatty acids. *Adv. Nutr.* 3:127–134. <https://doi.org/10.3945/an.111.001602>
- Hwang, S., X. Wang, R.M. Rodrigues, J. Ma, Y. He, W. Seo, S.H. Park, S.-J. Kim, D. Feng, and B. Gao. 2020. Protective and detrimental roles of p38 α mitogen-activated protein kinase in different stages of nonalcoholic fatty liver disease. *Hepatology*. 72:873–891. <https://doi.org/10.1002/hep.31390>
- Kersten, S., B. Desvergne, and W. Wahli. 2000. Roles of PPARs in health and disease. *Nature*. 405:421–424. <https://doi.org/10.1038/35013000>
- Khan, R.S., K. Drosatos, and I.J. Goldberg. 2010. Creating and curing fatty hearts. *Curr. Opin. Clin. Nutr. Metab. Care*. 13:145–149. <https://doi.org/10.1097/MCO.0b013e3283357272>
- Kim, S., I. Sohn, J.I. Ahn, K.H. Lee, Y.S. Lee, and Y.S. Lee. 2004. Hepatic gene expression profiles in a long-term high-fat diet-induced obesity mouse model. *Gene*. 340:99–109. <https://doi.org/10.1016/j.gene.2004.06.015>
- Lambert, J.E., and E.J. Parks. 2012. Postprandial metabolism of meal triglyceride in humans. *Biochim. Biophys. Acta*. 1821:721–726. <https://doi.org/10.1016/j.bbali.2012.01.006>
- Langsted, A., J.J. Freiberg, and B.G. Nordestgaard. 2008. Fasting and nonfasting lipid levels influence of normal food intake on lipids, lipoproteins, apolipoproteins, and cardiovascular risk prediction. *Circulation*. 118:2047–2056. <https://doi.org/10.1161/CIRCULATIONAHA.108.804146>
- Lawan, A., and A.M. Bennett. 2017. Mitogen-activated protein kinase regulation in hepatic metabolism. *Trends Endocrinol. Metab.* 28:868–878. <https://doi.org/10.1016/j.tem.2017.10.007>
- Lee, J., C. Sun, Y. Zhou, J. Lee, D. Gokalp, H. Herrema, S.W. Park, R.J. Davis, and U. Ozcan. 2011. P38 MAPK-mediated regulation of Xbpls is crucial for glucose homeostasis. *Nat. Med.* 17:1251–1260. <https://doi.org/10.1038/nm.2449>
- Li, S., M.S. Brown, and J.L. Goldstein. 2010. Bifurcation of insulin signaling pathway in rat liver: mTORC1 required for stimulation of lipogenesis, but not inhibition of gluconeogenesis. *Proc. Natl. Acad. Sci. USA*. 107: 3441–3446. <https://doi.org/10.1073/pnas.0914798107>
- Lignot, J.H., C. Helmstetter, and S.M. Secor. 2005. Postprandial morphological response of the intestinal epithelium of the Burmese python (*Python molurus*). *Comp. Biochem. Physiol. - A Mol. Integr. Physiol.* 141: 280–291. <https://doi.org/10.1016/j.cbpb.2005.05.005>
- Lonardo, A., S. Lombardini, M. Ricchi, F. Scaglioni, and P. Loria. 2005. Review article: Hepatic steatosis and insulin resistance. *Aliment. Pharmacol. Ther.* 22:64–70. <https://doi.org/10.1111/j.1365-2036.2005.02600.x>
- Magida, J.A., and L.A. Leinwand. 2014. Metabolic crosstalk between the heart and liver impacts familial hypertrophic cardiomyopathy. *EMBO Mol. Med.* 6:482–495. <https://doi.org/10.1002/emmm.201302852>
- Menni, C., E. Fauman, I. Erte, J.R.B. Perry, G. Kastenmüller, S.Y. Shin, A.K. Petersen, C. Hyde, M. Psatha, K.J. Ward, et al. 2013. Biomarkers for type 2 diabetes and impaired fasting glucose using a nontargeted metabolomics approach. *Diabetes*. 62:4270–4276. <https://doi.org/10.2337/db13-0570>
- Passonneau, J.V., and V.R. Lauderdale. 1974. A comparison of three methods of glycogen measurement in Tissues. *Anal. Biochem.* 60:405–412. [https://doi.org/10.1016/0003-2697\(74\)90248-6](https://doi.org/10.1016/0003-2697(74)90248-6)
- Petersen, K.F., S. Dufour, D. Befroy, M. Lehrke, R.E. Hendler, and G.I. Shulman. 2005. Reversal of nonalcoholic hepatic steatosis, hepatic insulin resistance, and hyperglycemia by moderate weight reduction in patients with type 2 diabetes. *Diabetes*. 54:603–608. <https://doi.org/10.2337/diabetes.54.3.603>
- Prati, D., E. Taioli, A. Zanella, E.D. Torre, S. Butelli, D. E.D. Vecchio, L. Vianello, F. Zanuso, F. Mozzi, S. Milani, et al. 2002. Updated definitions of healthy ranges for serum alanine aminotransferase levels. *Ann. Intern. Med.* 137:1–10. <https://doi.org/10.7326/0003-4819-137-1-200207020-00006>

- Riquelme, C.A., J.A. Magida, B.C. Harrison, C.E. Wall, T.G. Marr, S.M. Secor, and L.A. Leinwand. 2011. Fatty acids identified in the Burmese python promote beneficial cardiac growth. *Science*. 334:528–531. <https://doi.org/10.1126/science.1210558>
- Rius-Pérez, S., A.M. Tormos, S. Pérez, I. Finamor, P. Rada, M.Á. Valverde, A.R. Nebreda, J. Sastre, and R. Taléns-Visconti. 2019. p38 α deficiency restrains liver regeneration after partial hepatectomy triggering oxidative stress and liver injury. *Sci. Rep.* 9:3775. <https://doi.org/10.1038/s41598-019-39428-3>
- Secor, S.M. 2008. Digestive physiology of the Burmese python: Broad regulation of integrated performance. *J. Exp. Biol.* 211:3767–3774. <https://doi.org/10.1242/jeb.023754>
- Secor, S.M., and J. Diamond. 1995. Adaptive responses to feeding in Burmese pythons: Pay before pumping. *J. Exp. Biol.* 198:1313–1325. <https://doi.org/10.1242/jeb.198.6.1313>
- Secor, S.M., and J. Diamond. 1997. Effects of meal size on postprandial responses in juvenile Burmese pythons (*Python molurus*). *Am. J. Physiol.* 272:R902–R912. <https://doi.org/10.1152/ajpregu.1997.272.3.R902>
- Secor, S.M., and J. Diamond. 1998. A vertebrate model of extreme physiological regulation. *Nature*. 395:659–662. <https://doi.org/10.1038/27131>
- Smith, G.I., M. Shankaran, M. Yoshino, G.G. Schweitzer, M. Chondronikola, J.W. Beals, A.L. Okunade, B.W. Patterson, E. Nyangau, T. Field, et al. 2020. Insulin resistance drives hepatic de novo lipogenesis in nonalcoholic fatty liver disease. *J. Clin. Investig.* 130:1453–1460. <https://doi.org/10.1172/JCI134165>
- Teupser, D., S. Pavlides, M. Tan, J.C. Gutierrez-Ramos, R. Kolbeck, and J.L. Breslow. 2004. Major reduction of atherosclerosis in fractalkine (CX3CL1)-deficient mice is at the brachiocephalic artery, not the aortic root. *Proc. Natl. Acad. Sci. USA*. 101:17795–17800. <https://doi.org/10.1073/pnas.0408096101>
- Vatner, D.F., S.K. Majumdar, N. Kumashiro, M.C. Petersen, Y. Rahimi, A.K. Gattu, M. Bears, J.P.G. Camporez, G.W. Cline, M.J. Jurczak, et al. 2015. Insulin-independent regulation of hepatic triglyceride synthesis by fatty acids. *Proc. Natl. Acad. Sci. USA*. 112:1143–1148. <https://doi.org/10.1073/pnas.1423952112>
- Vergara, D., A. Casadei-Gardini, and A.M. Giudetti. 2019. Oxidative molecular mechanisms underlying liver diseases: From systems biology to the personalized medicine. *Oxid. Med. Cell. Longev.* 2019:7864316. <https://doi.org/10.1155/2019/7864316>
- Wada, T., H. Kenmochi, Y. Miyashita, M. Sasaki, M. Ojima, M. Sasahara, D. Koya, H. Tsuneki, and T. Sasaoka. 2010. Spironolactone improves glucose and lipid metabolism by ameliorating hepatic steatosis and inflammation and suppressing enhanced gluconeogenesis induced by high-fat and high-fructose diet. *Endocrinology*. 151:2040–2049. <https://doi.org/10.1210/en.2009-0869>
- Wall, C.E., S. Cozza, C.A. Riquelme, W.R. McCombie, J.K. Heimiller, T.G. Marr, and L.A. Leinwand. 2011. Whole transcriptome analysis of the fasting and fed Burmese python heart: Insights into extreme physiological cardiac adaptation. *Physiol. Genom.* 43:69–76. <https://doi.org/10.1152/physiolgenomics.00162.2010>
- Weltman, M.D., G.C. Farrell, and C. Liddle. 1996. Increased hepatocyte CYP2E1 expression in a rat nutritional model of hepatic steatosis with inflammation. *Gastroenterology*. 111:1645–1653. [https://doi.org/10.1016/s0016-5085\(96\)70028-8](https://doi.org/10.1016/s0016-5085(96)70028-8)
- Xia, J., I.V. Sinelnikov, B. Han, and D.S. Wishart. 2015. MetaboAnalyst 3.0—making metabolomics more meaningful. *Nucleic Acids Res.* 43:W251–W257. <https://doi.org/10.1093/nar/gkv380>
- Yoon, J.C., P. Puigserver, G. Chen, J. Donovan, Z. Wu, J. Rhee, G. Adelmant, J. Stafford, C.R. Kahn, D.K. Granner, et al. 2001. Control of hepatic gluconeogenesis through the transcriptional coactivator PGC-1. *Nature*. 413:131–138. <https://doi.org/10.1038/35093050>

Supplemental material

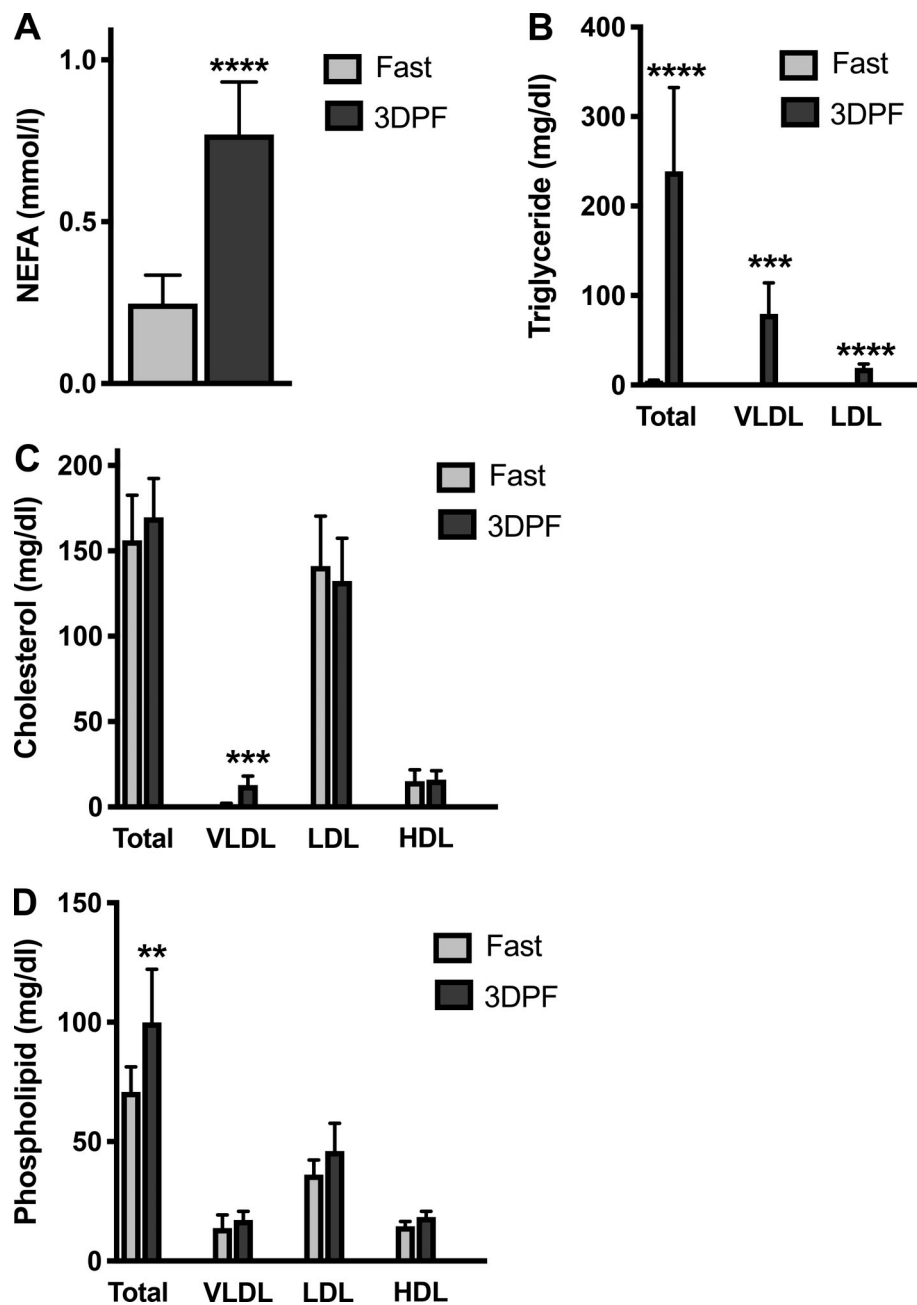
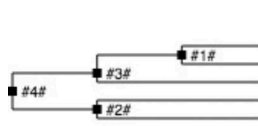


Figure S1. **Levels of NEFA, TG, cholesterol, and phospholipid in fasted and 3DPF pythons.** Levels of cholesterol content in Burmese python plasma. **(A)** Levels of NEFAs in fasted and 3DPF pythons. **(B)** Levels of triglycerides in fasted and 3DPF pythons. **(C)** Levels of cholesterol in fasted and 3DPF pythons. **(D)** Levels of phospholipids in fasted and 3DPF pythons. **, $P \leq 0.01$; ***, $P \leq 0.001$; ****, $P \leq 0.0001$.

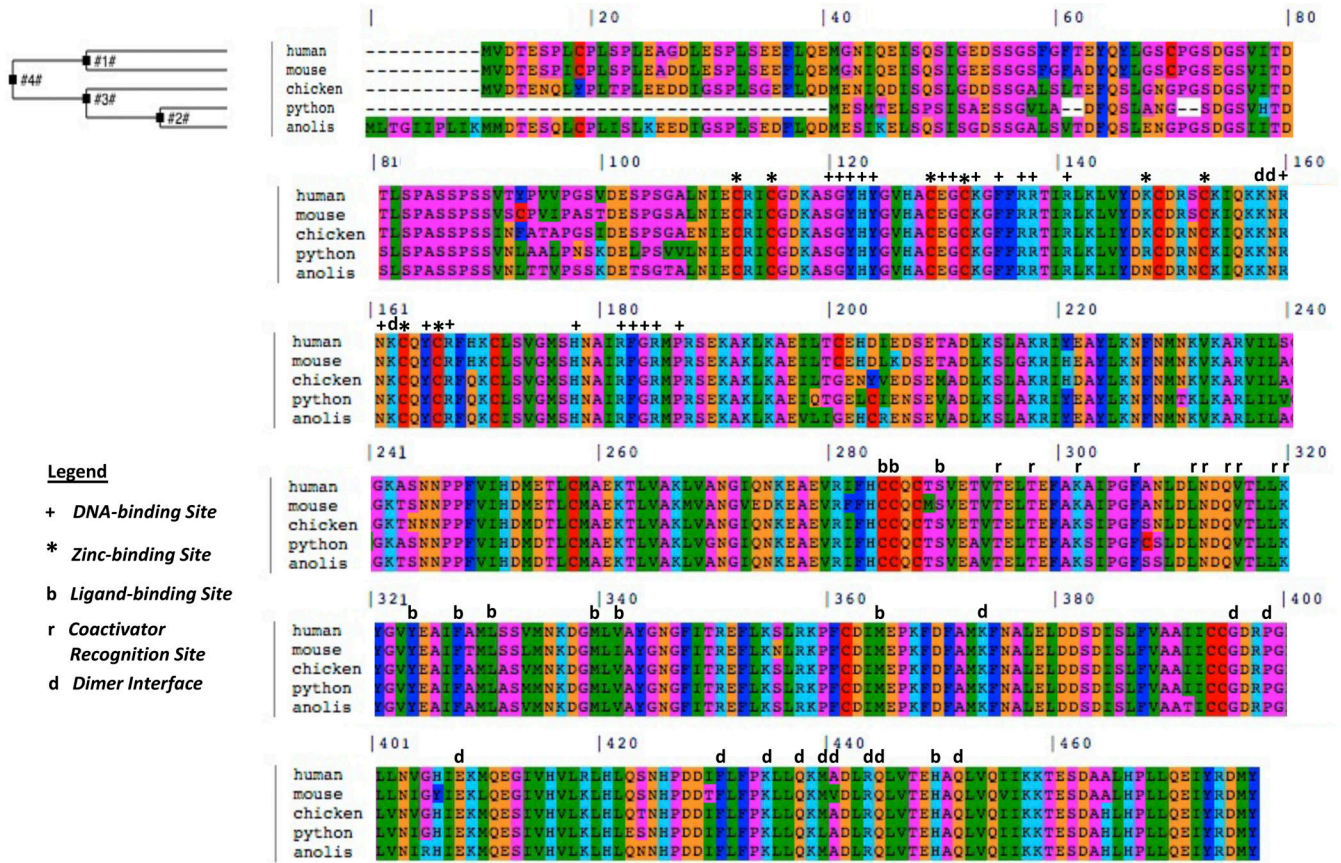


Legend

- + DNA-binding Site
- * Zinc-binding Site
- b Ligand-binding Site
- r Coactivator Recognition Site
- d Dimer Interface



Figure S2. Alignment of FXR orthologs using EMBL-EBI webPRANK alignment of *Python molurus bivittatus*-5.0.2 (NW_006532574.1). FXR sequence comparison between Burmese python and other species. FXR ortholog sequences are aligned between mouse, human, chicken, anolis, and python using EMBL-EBI webPRANK alignment of *Python molurus bivittatus*-5.0.2 (NW_006532574.1).



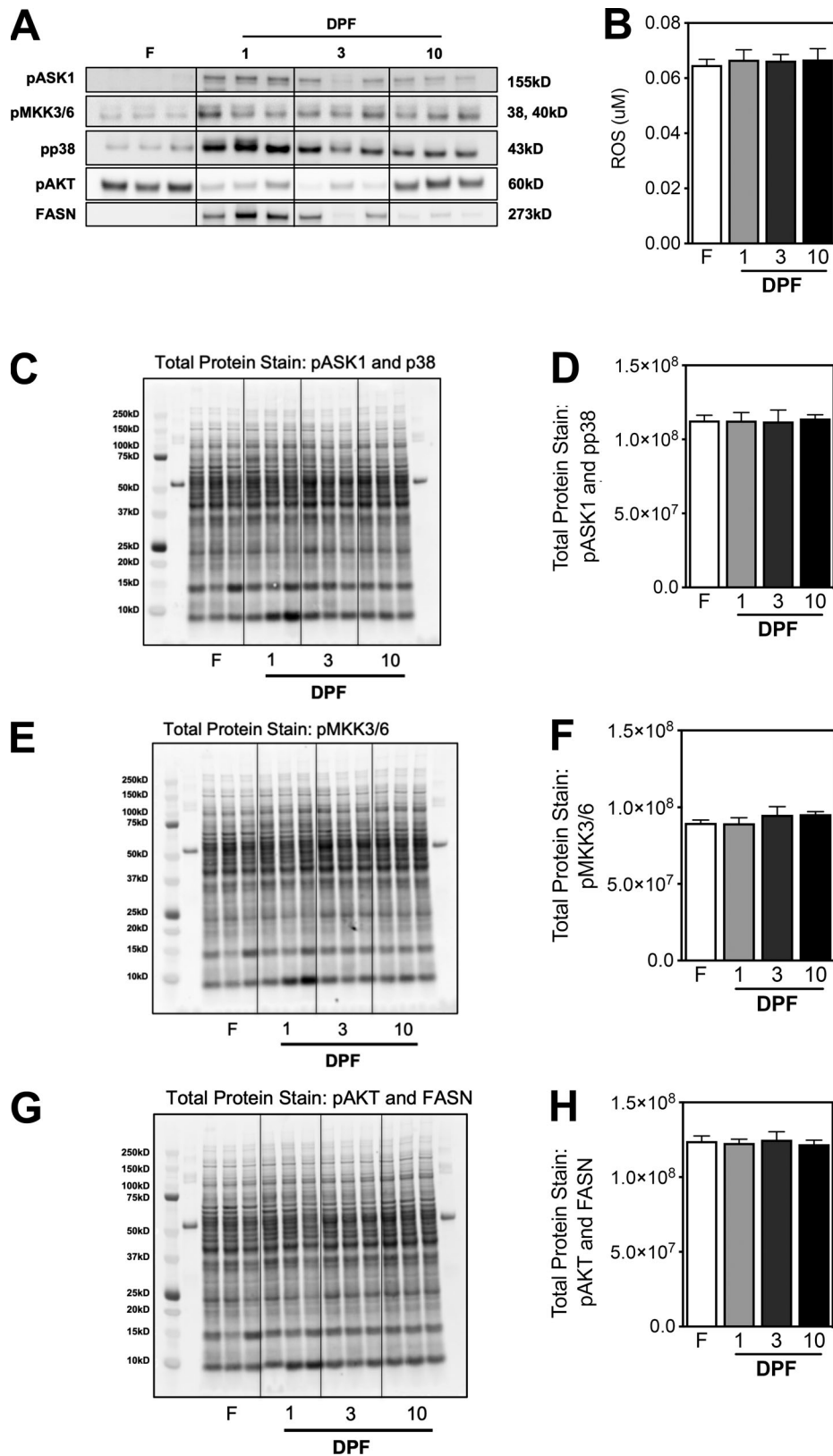


Figure S4. **Western blots used for quantitative analysis and normalization.** (A) Western blot used for quantitative analysis of pASK1, pMKK3/6, pp38, pAKT, and FASN. (B) ROS level, quantitative analysis. (C and D) Western blot total protein stain used for normalization of pASK1 and pp38. (E and F) Western blot total protein stain used for normalization of pMKK3/6. (G and H) Western blot total protein stain used for normalization of pAKT and FASN. Source data are available for this figure: SourceData F54.

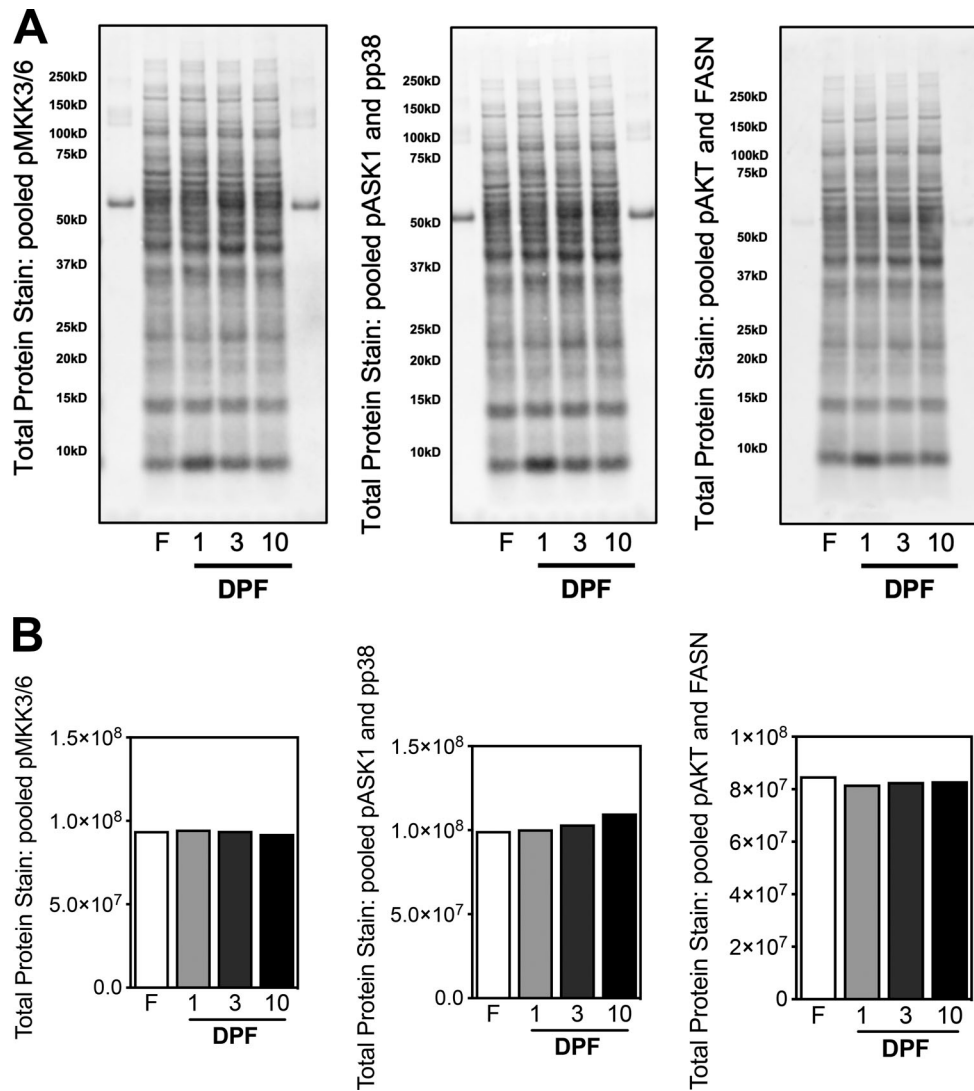


Figure S5. **Western blots used for representative blots. (A and B)** Western blot total protein stain of representative blots showed in Fig. 5 A. Source data are available for this figure: SourceData FS5.

Provided online are Table S1 and Table S2. Table S1 lists the top 10 conserved domain hits for python FXR and PPAR α orthologs, analyzed by NCBI CD Search. Table S2 lists sequences of primers used for RT-PCT in python liver.